Validation of High-Order Wall-Resolved Large-Eddy Simulation of Vertical-Axis Wind Turbines

Samuel Kanner*, and Per-Olof Persson†

University of California, Berkeley, Berkeley, CA 94720-3840, U.S.A.

A high-order Wall-Resolved Implicit Large Eddy Simulation (WR-ILES) method is used to simulate a vertical-axis wind turbine in 2D and 3D. In this work, we perform these simulations at nearly full-scale Reynolds numbers ($\mathcal{O}(10^5)$). The high-order simulations are compared to experimental wind tunnel data, where the turbine blades were outfitted with pressure sensors. The wind turbine is also simulated with a low-order, finite volume method found in OpenFOAM. The results of tangential forces are compared and it is shown that both methods adequately estimate the forces in the upwind section of the blade. The flow structure at various time instances is shown in 2D and 3D.

I. Introduction

Vertical-axis wind turbines (VAWTs) fell out of favor during the development of the wind energy industry at the end of the twentieth century due to their inferior efficiency, reliability and structural integrity as compared to their horizontal-axis counterparts. One of the major issues in the design of the turbine and its support structure is the prediction of the unsteady, aerodynamic loads. Considering only a single revolution under normal operating conditions, the blades of a horizontal-axis wind turbine (HAWT) do not experience drastic changes in the angle of attack, since their planar orientation relative to the incident wind remains unchanged. The blades of a VAWT, however, undergo large changes in angle of attack, the severity of which is determined by the tip-speed ratio (TSR). As a blade undergoes a single revolution, the angle of attack may vary by as much as 50-60°. For nearly all airfoil shapes, especially symmetric airfoils which are commonly used on VAWTs, these changes in angle of attack correspond to the blade undergoing phenomenon of dynamic stall. When dynamic stall occurs, the flow detaches from the suction side of airfoil and the nature of the flow field and forces on the airfoil becomes much more difficult to predict. Many of the VAWTs built in the 1970s-1980s suffered fatigue damage due to these cyclic stresses and the fact that many were built out of aluminum (instead of fiberglass, which is more commonly used today).[1] Recent renewed interest has come to the field of vertical-axis wind turbines as the possibility of floating wind turbines continue to grow (see Refs. 2–5). Clearly, throughout the development and commercialization of wind turbines over the past half-century the focus was on onshore operation. Although the industry is successfully moving to implement HAWTs on floating structures,[6] the following characteristics of VAWTs make them attractive to designers of floating platforms:

1. For a given power rating, the center of thrust of the rotor of a VAWT is located midway on the span of the blades, reducing the overtopping moment on the platform.

2. The vertical center of gravity of a VAWT is located near the deck of the platform, due to the fact that generator, yaw and pitch motors and other drivetrain components are located on the platform deck.

3. Generally, the planar accelerations of a nacelle of a VAWT are relatively small since it is located on or near the platform deck. Since most wind turbines and components have limits on the nacelle accelerations, this feature can lead to a high availability factor of a VAWT.

*Previously Ph.D. student at UC Berkeley. Currently R&D Team, Principle Power Incorporated, Emeryville CA 94608. E-mail: skanner@principlepowerinc.com. AIAA Member.

†Associate Professor, Department of Mathematics, University of California, Berkeley, Berkeley CA 94720-3840. E-mail: persson@berkeley.edu. AIAA Senior Member.

4. The generator and drivetrain components are easily accessible on a VAWT since they are located on the platform deck. Due to the complex nature of offshore operations, which must be scheduled around certain weather windows, the possibility of reduced downtime can also improve the availability factor of a VAWT.

For these reasons, a number researchers are re-examining ways of improving the efficiency of vertical-axis wind turbines, with an eye towards floating platforms.[5,7,8]

Continued research has been performed for small-scale land-based VAWTs. This type of research and development must occur before the turbines are located on offshore platforms where operation, maintenance and monitoring activities are all more complex. In order to validate numerical tools used in analyzing unsteady, aerodynamic forces on VAWT airfoils, results from wind tunnel tests can be compared to simulations. One of the issues with model tests is that they occur at a smaller Reynolds number than what might occur for a large-scale wind turbine. A simulation technique which may be accurately predicting the unsteady airflow and airfoil forces at a certain Reynolds number may not do so at another. This effect is particularly true in methods for computational fluid dynamics, where the mesh size, wall models and type of solver all depend on the properties of the fluid flow, such as the Reynolds number.

In this paper, we validate a wall-resolved implicit large eddy simulation technique using experimental data from a test campaign, documented in many papers.[9–11] In these larger-scale wind tunnel tests, the Reynolds number exceeded 10^5. This type of ILES technique was validated at lower Reynolds previously[12] and was compared to tests of a VAWT in a tow tank. These wind tunnel tests are performed at a Reynolds number one order of magnitude higher. The higher-order method is also compared to a low-order finite volume method found in the popular, open-source software, OpenFOAM. The paper is organized into a numerical approach, results and discussion sections. First, the mathematical model and governing equations of the large eddy simulation technique are described. The framework of the finite volume methodology is also briefly introduced. Second, the computational domain and experimental VAWT turbine in Ref. [9] is shown. Third, the results of various validation studies using this turbine are presented. The parameters include, solidity, tip-speed ratio and toe-out angle. Finally, a discussion on the advantages and drawbacks of the various computational methods is offered.

II. Numerical Approach

A. High-Order, Finite Element Method

Our simulations are based on an artificial compressibility formulation of the Navier-Stokes equations, which can approximate nearly incompressible flows well.[13] The governing equations are derived from the compressible equations by introducing an artificial equation of state,[14] which we define by an isentropic assumption defined in terms of an artificial Mach number M. This results in a system of equations in the conserved variables ρ (density) and $\rho\boldsymbol{u}$ (momentum). We impose two types of boundary conditions, free-stream flow (far field) and prescribed velocity (wall).

1. Arbitrary-Lagrangian-Eulerian (ALE) Framework

We denote the time-varying domain as $\boldsymbol{v}(t) \in \mathbb{R}^n$ and consider the governing equations of the compressible isentropic flow in $\boldsymbol{v}(t)$ as a system of conservation laws,

$$\frac{\partial \boldsymbol{u}}{\partial t} + \nabla \cdot \boldsymbol{f}(\boldsymbol{u}, \nabla \boldsymbol{u}) = 0 \tag{1}$$

where $\boldsymbol{u}$ is the vector of conserved variables and $\boldsymbol{f}$ is the flux function. The ALE formulation then chooses a fixed reference domain as V, and constructs a smooth mapping $\boldsymbol{\mathcal{G}}(\boldsymbol{X}, t) : \boldsymbol{V} \to \boldsymbol{v}(t)$ between the reference domain and the moving domain. Based on this mapping, we define the deformation gradient $\boldsymbol{G}$, mapping velocity $\boldsymbol{v_X}$ and mapping Jacobian g as

$$\boldsymbol{G} = \nabla_{\boldsymbol{X}} \boldsymbol{\mathcal{G}}, \;\; \boldsymbol{v_X} = \frac{\partial \boldsymbol{\mathcal{G}}}{\partial t}, \;\; g = \det \boldsymbol{G}. \tag{2}$$

Using these quantities, we can rewrite the conservation law (1) as a new system in the domain V,

$$\frac{\partial \boldsymbol{U}}{\partial t} + \nabla_{\boldsymbol{X}} \cdot \boldsymbol{F}(\boldsymbol{U}, \nabla_{\boldsymbol{X}} \boldsymbol{U}) = 0 \tag{3}$$

with new solution vector $\boldsymbol{U}$ and new flux functions $\boldsymbol{F}$. In this work, all our mappings $\boldsymbol{\mathcal{G}}(\boldsymbol{X}, t)$ are rigid rotations around the center of the turbine, which results in a simple implementation which does not need sophisticated mesh deformation algorithms. We refer to Ref. 15 for more details on this ALE formulation.

2. Discontinuous Galerkin Discretization

The system (3) is discretized in space using a high-order accurate discontinuous Galerkin method.[16,17] We split the flux function into an inviscid and a viscous part according to $\boldsymbol{F}(\boldsymbol{U}, \nabla_{\boldsymbol{X}}\boldsymbol{U}) = \boldsymbol{F}^{\text{inv}}(\boldsymbol{U}) + \boldsymbol{F}^{\text{vis}}(\boldsymbol{U}, \nabla_{\boldsymbol{X}}\boldsymbol{U})$. For the numerical fluxes in the boundary integrals, we use Roe's method[18] to approximate the inviscid flux and we treat the viscous flux using the Compact Discontinuous Galerkin (CDG) method.[19] This discretization leads to a (large) non-linear system of ordinary differential equations, which we solve using a fully coupled high-order implicit Runge-Kutta (IRK) method.[20] In this work, we use polynomial degrees of order $p = 3$ for the spatial discretization, and a 2-stage, 3rd order accurate IRK method for the temporal discretization. The systems of equations that arise in these implicit solvers are solved using a parallel preconditioned Newton-Krylov method.[21]

B. Low-order, Finite Volume Method

The methodology briefly presented herein represents the incompressible Navier-Stokes equations in OpenFOAM.[22] For more detailed information on the equations and algorithms, see Ref. [23]. A form of the incompressible Navier-Stokes is,

$$\frac{\partial \mathbf{U}}{\partial t} = -\nabla \cdot (\mathbf{U} \otimes \mathbf{U}) - \nabla \cdot \tau_{\mathbf{inco}} - \nabla \frac{\mathbf{p}}{\rho} + \mathbf{g}. \tag{4}$$

The conservation of mass statement found in the continuity equation for incompressible flow is commonly written as,

$$\nabla \cdot \mathbf{U} = \mathbf{0}. \tag{5}$$

Thus, there are four unknowns, U_x, U_y, U_z and p and four equations. To solve these coupled equations, an algorithm known as `PIMPLE` is employed, which solves for the unknowns sequentially. The algorithm is a merged form of the `PISO` and `SIMPLE` algorithms, which are briefly described. The `SIMPLE` algorithm, or Semi-Implicit-Method-Of-Pressure-Linked-Equations assumes the solution is steady-state. An implementation of the `SIMPLE` algorithm, known as the `SIMPLEC` algorithm is currently employed in OpenFOAM.[24] The `PISO` algorithm, or Pressure-Implicit-Split-Operator algorithm is employed for transient calculations. In this algorithm, the CFL number has the usual restriction that it cannot go above unity. In the `PIMPLE` algorithm, however, this condition is relaxed. In a given time-step the `SIMPLE` algorithm is used to find a steady-state solution with under-relaxation. Then the `PISO` algorithm is employed to solve the explicit parts of the equations using a predictor-corrector algorithm.[25]

In the work presented herein, the solution method `PimpleDyMFOAM` is utilized. This method generalizes the `PIMPLE` method to a case with a dynamic mesh. In these simulations, the entire domain is rotated using a prescribed rotation rate that ramps to the desired ω. Only the solution after the domain is spinning at the desired ω is used. Other techniques for rotating frames were attempted, such as the Multiple Reference Frame (MRF) technique. However, it was found that these techniques led to non-physical wakes.

Two types of wall models are used in order to compare to the high-order simulations. The first technique does not include any wall model to attempt to recreate the conditions in the high-order method employed for this study (wall-resolved). Thus, the OpenFOAM turbulence model is set to *laminar*. In Sec. IV, this is known as the base OpenFOAM model. Another simulation technique with an LES wall model was employed where the dynamic k-equation turbulence model was used. In Sec. IV, this is known as the OpenFOAM-LES model.

III. Geometry

A. Model-Scale Turbine

The model turbine is shown in Fig. 1. A large wind tunnel at Mie University in Japan was utilized to perform the wind tunnel tests. The test section is 4.5m x 4.5m and the incident wind can be adjusted from 0-30 m/s.[10] The turbulence is less than 1.2% in the mainstream direction when the experiment is at 8.0 m/s. The

turbine consists of 2-5 blades, with a height H of 1.2m. The airfoil shape is a symmetric NACA0021, with a chord length of 0.265m. Other geometric parameters are shown in Table 1. To measure the aerodynamic forces and torque on the turbine, two different techniques were employed. The first technique involved the installation of pressure taps around the blade at certain heights. Further details on the pressure sensors used and calibration can be found in Ref. 10. The second measurement technique involved using a six-component balance, shown as the base in Fig. 1. This balance appears to be measuring the reaction force of the VAWT support structure with respect to the ground. Thus, the torque measurement at this point in the power conversion chain includes frictional losses between the rotor and VAWT body. The losses on the model turbine are quite large, generally between 25-50% depending on the solidity and tip-speed ratio (see Fig. 19 in Ref. 10). Strangely, the losses appear to be inversely correlated with tip-speed ratio, which would contradict a linear or quadratic drag model between the rotor and VAWT body.

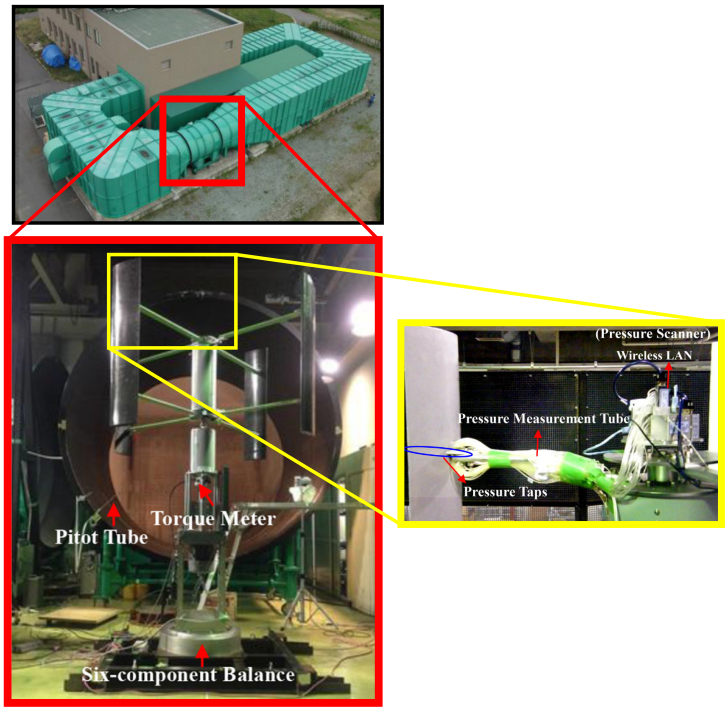

Figure 1. Photographs from experimental setup, adapted from Ref. 10. Top photograph shows large-scale wind tunnel at Mie University in Japan. Middle photograph shows experimental turbine and right photograph shows one of the blades outfitted with pressure sensors.

Parameter	Value	Unit
c	0.265	m
c_0	$0.25c$	m
R	1.0	m
λ	1.8	-
N_b	3	-
H	1.2	m
U_0	8.0	m/s
α_0	6	deg

Table 1. Geometry of the full-scale VAWT considered in this study. See Fig. 2 for definitions of geometric variables.

B. Computational Domain

A generic two-bladed VAWT is shown in plan view in Fig. 2. Many geometric definitions of the VAWT are shown, including instantaneous angle of attack α, blade offset pitch angle α_0, chord length c, blade offset distance c_0, VAWT radius R, azimuthal angle θ, and VAWT angular velocity ω. The inflow velocity from the left is constant $U_0 = 8m/s$. From these parameters we form the common non-dimensional rotational speed ratio, known as the tip-speed ratio as,

$$\lambda = \frac{\omega R}{U_0} \tag{6}$$

The domain is commonly divided into the upwind and downwind zones as depicted in Fig. 2. It is well

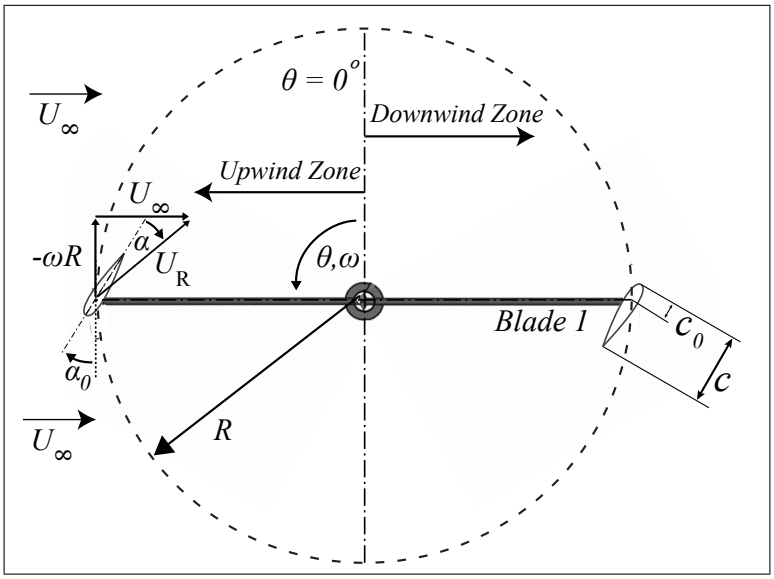

Figure 2. Plan view of 2-bladed VAWT with definitions of angle of attack α, blade offset pitch angle α_0, chord length c, blade offset distance c_0, VAWT radius R, azimuthal angle θ, and VAWT angular velocity ω.

known that structure of the VAWT, including the central tower and radial struts, which are not modeled in these CFD simulations can disturb the flow, increasing the difficulty of predicting the flow in the downwind zone.

C. Meshes

Our finite element and finite volume methods are capable of handling arbitrary meshes of a variety of elements. We use quadrilateral meshes for our 2D simulations, which are extruded to hexahedral elements for the 3D simulations. The refinements in the boundary layers are generated by an anisotropic splitting procedure. The resulting high-order 2D mesh is shown in Fig. 3. This mesh of a 3-bladed turbine has 3,847 quadrilateral elements of degree $p = 3$, leading to a total number of high-order nodes of 61,552 (blue dots in the figure), and a total number of DOFs of about 185,000. The right figure also shows the corresponding low-order mesh, which we use for the OpenFOAM simulations. This mesh is chosen such that it has exactly the same number of degrees of freedom as the high-order mesh (by refining the high-order elements uniformly twice).

For the 3D simulations, we extrude this mesh in the z-direction to generate 6 layers of high-order hexahedral elements (see Fig. 4). The resulting mesh consists of about 23,000 hexahedral elements of degree $p = 3$, or about $620,000$ high-order nodes and 2.5 million total DOFs.

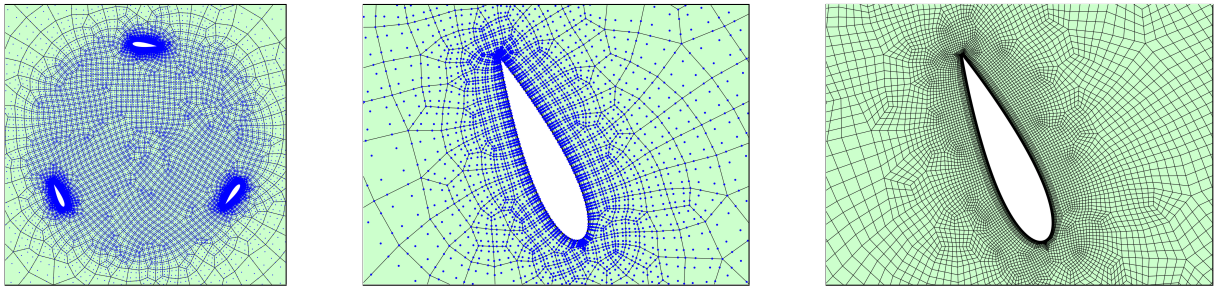

Figure 3. A 3-bladed mesh used for the high-order 2D simulations. The blue does in the two left pictures show the high-order nodes. The right plot shows the corresponding low-order mesh, which has the same number of degrees of freedom.

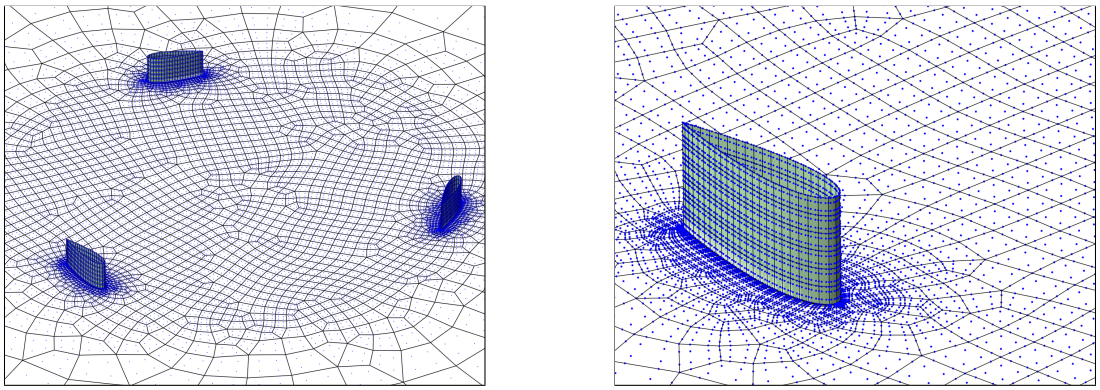

Figure 4. 3D hexahedral mesh for the 3-bladed turbine.

IV. Results

To explore the efficiency of the turbines the tangential force on each airfoil of the turbines is calculated. The sectional tangential force coefficient is defined as,

$$C_T(\theta) = \frac{F_T(\theta)}{1/2\rho U_\infty^2 c} \tag{7}$$

where F_T is the sectional tangential force of a representative blade on the wind turbine. In 3D, the tangential force coefficient is normalized by the length of the span of the 3D blade. The tangential force coefficient is shown in Fig. 5 as a function of azimuthal angle for $\lambda = 1.8$. The thin, colored lines show the coefficients for each of the three blades in 2D, averaged over 2 revolutions. The thick gray line is the average tangential coefficient in 2D, which is the average of these curves. The thicker line with circular markers shows the average tangential coefficients for the 3D turbine and the triangular markers show the experimental data.

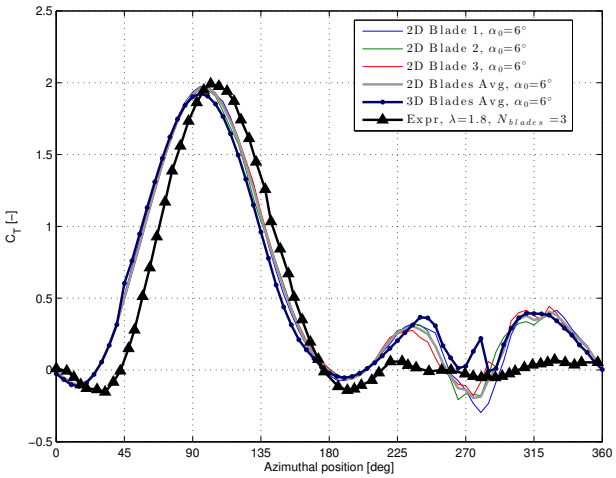

Figure 5. Tangential force coefficient as a function of azimuthal angle for $\lambda = 1.8$ for the WR-ILES simulations as compared to the experimental data.[10]

A. Torque Comparison

A comparison between the two simulation techniques is shown in Fig. 6. The total OpenFOAM solution is shown in red and fairly closes matches the experimental data in the upwind zone ($0° \leq \theta \leq 180°$). However, in the downwind zone ($0° < \theta \leq 360°$), the OpenFOAM calculation drastically overpredicts the force coefficient. Hence the addition of the viscous forces to just the pressure solution (blue line) causes a reduction in the efficiency. The wall-resolved ILES results are shown in gray and dark blue for comparison.

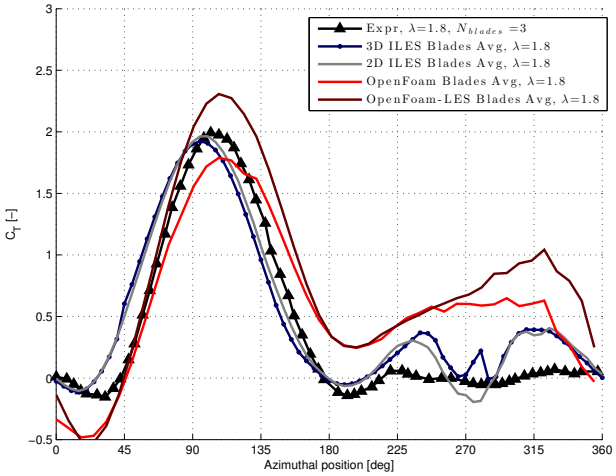

Figure 6. Tangential force coefficients as a function of azimuthal angle for the high-order and low-order methods considered in this study. Both results are compared to experimental data.[10]

B. Flow Visualization

The vorticity of the flow field are calculated from the solutions of each simulation technique. Figure 7 shows the vorticity of the ILES solution in the left column and the OpenFOAM solution in the right column. The OpenFOAM solutions with and without the LES wall model showed similar vortical structures in the flow field at these time instances. The rows indicate different azimuthal positions of Blade 1: 0°, 90°, 180°, 270°. The OpenFOAM simulations are shown after 2 revolutions of the turbine, while the ILES solution has only undergone 1 full revolution. From the time history of the forces on the blades, it was apparent that forces settled into a cyclic response after 1-2 revolutions. It is clear from Fig. 7 that the low-order, finite volume

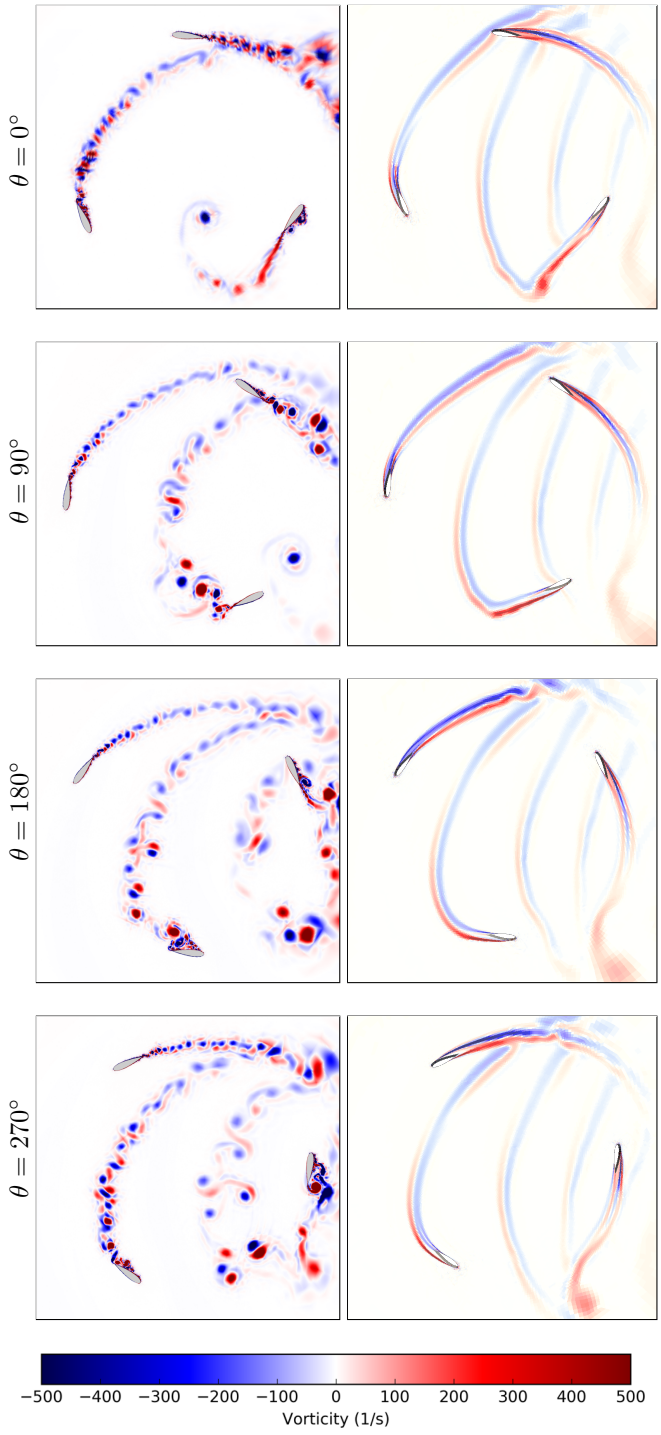

Figure 7. Instantaneous snapshots of the vorticity of the fluid domain with high-order, finite element CFD method in left column and low-order, finite volume CFD method in right column.

method does not capture the vortical nature of the flow field as well as the high-order method, even though the meshes have the same number of degrees of freedom.

An illustration of the flow field in our 3D simulations is shown in Fig. 8. It is clear from these isosurfaces of the kinetic energy that the flow is highly separated and unsteady. Still, we note that in the torque plots the 2D results are quite comparable.

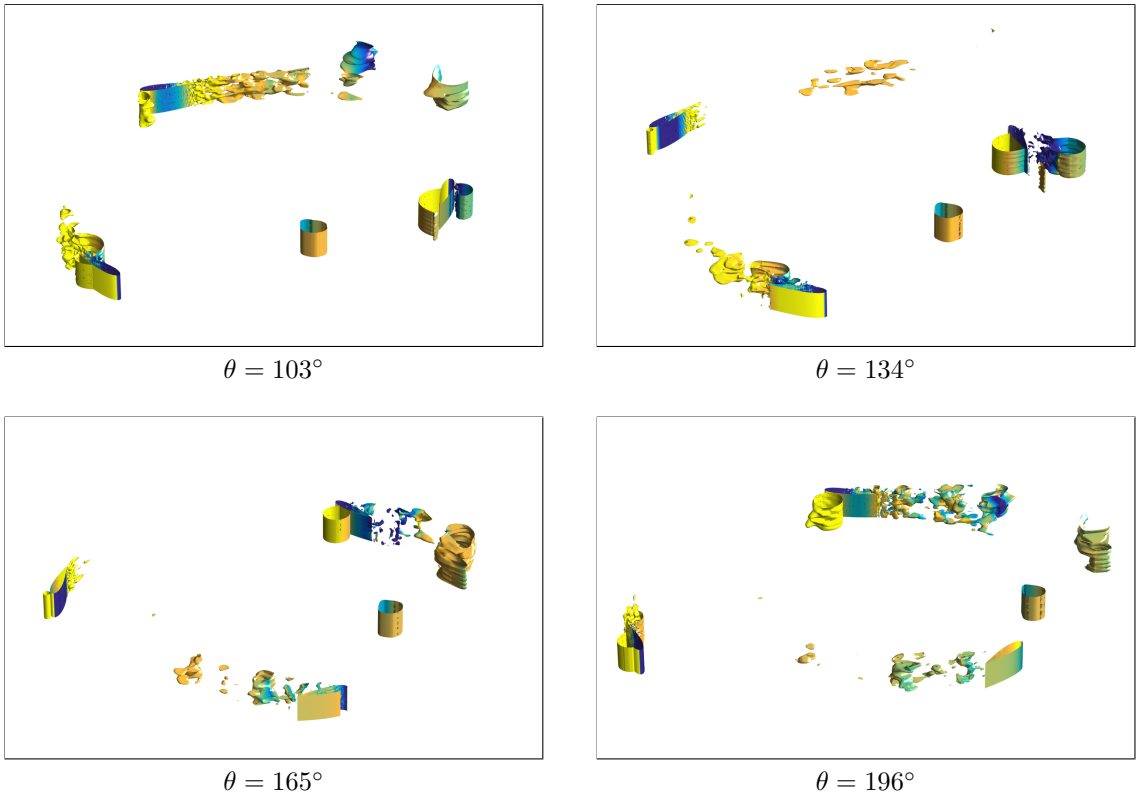

Figure 8. Flow field for the 3D simulation of the 3-bladed turbine. Isosurfaces of the kinetic energy are shown, colored by the pressure field.

V. Conclusions

A wall-resolved, implicit large eddy simulation (WR-ILES) technique was employed to study the behavior of a vertical-axis wind turbine at large Reynolds number ($Re > 10^5$). A low-order, finite volume method utilized in the open-source software OpenFOAM was also used to study the same problem. The results show that both codes predict the torque on the turbine in the upwind section. However, the high-order simulation technique makes a more accurate estimation of the airfoil forces in the downwind section. Both software suffer from the simplistic geometry of the computational domain. The central rotor and struts were not modeled. Furthermore, as shown in Fig. 1, there were numerous tubes running from the airfoil to the central column for pressure sensing and data processing. These tubes may have an undue effect on the airflow in the downstream section, especially. It was confirmed that for this geometry the 2D results generally follow the 3D results. Visualizing the unsteady flow in the computational domain, the dissipative nature of the low-order method was apparent.

In the future, the central rotor and struts should be modeled in the 3D computational domain. Results presented in Ref. 26 indicate that there are significant changes in the pressure distribution power coefficient calculation along the spanwise direction of the turbine blade. Furthermore, these simulation techniques should also be used to predict the forces and flow fields for the various turbines used in Ref. 26 and 10 at different tip-speed ratios.

Acknowledgments

This research used resources of the National Energy Research Scientific Computing Center, a DOE Office of Science User Facility supported by the Office of Science of the U.S. Department of Energy under Contract No. DE-AC02-05CH11231.

References

[1]McGowan, J. G. and Connors, S. R., "WINDPOWER: A Turn of the Century Review," *Annual Review of Energy and the Environment*, Vol. 25, No. 1, 2000, pp. 147–197.

[2]Bull, D. L., Fowler, M., and Goupee, A., "A Comparison of Platform Options for Deep-water Floating Offshore Vertical Axis Wind Turbines: An Initial Study." Tech. rep., Sandia National Laboratories (SNL-NM), Albuquerque, NM (United States), 2014.

[3]Borg, M. and Collu, M., "A comparison between the dynamics of horizontal and vertical axis offshore floating wind turbines," *Philosophical Transactions of the Royal Society A: Mathematical, Physical and Engineering Sciences*, Vol. 373, No. 2035, 2015, pp. 20140076.

[4]Borg, M. and Collu, M., "Offshore floating vertical axis wind turbines, dynamics modelling state of the art. Part III: Hydrodynamics and coupled modelling approaches," *Renewable and Sustainable Energy Reviews*, Vol. 46, June 2015, pp. 296–310.

[5]Kanner, S., *Design, Analysis, Hybrid Testing and Orientation Control of a Floating Platform with Counter-Rotating Vertical-Axis Wind Turbines*, Ph.D. thesis, University of California, Berkeley, 2015.

[6]Roddier, D., Cermelli, C., Aubault, A., and Weinstein, A., "WindFloat: A floating foundation for offshore wind turbines," *Journal of Renewable and Sustainable Energy*, Vol. 2, No. 3, June 2010, pp. 033104.

[7]Owens, B. C., Hurtado, J. E., Paquette, J. A., Griffith, D. T., and Barone, M., "Aeroelastic Modeling of Large Offshore Vertical-axis Wind Turbines: Development of the Offshore Wind Energy Simulation Toolkit," 2014.

[8]Sutherland, H. J., Berg, D. E., and Ashwill, T. D., "A retrospective of VAWT technology," *Sandia National Laboratories*, 2012.

[9]Li, Q., Maeda, T., Kamada, Y., Murata, J., Yamamoto, M., Ogasawara, T., Shimizu, K., and Kogaki, T., "Study on power performance for straight-bladed vertical axis wind turbine by field and wind tunnel test," *Renewable Energy*, Vol. 90, No. Supplement C, May 2016, pp. 291–300.

[10]Li, Q., Maeda, T., Kamada, Y., Murata, J., Furukawa, K., and Yamamoto, M., "Effect of number of blades on aerodynamic forces on a straight-bladed Vertical Axis Wind Turbine," *Energy*, Vol. 90, No. Part 1, Oct. 2015, pp. 784–795.

[11]Li, Q., Maeda, T., Kamada, Y., Murata, J., Shimizu, K., Ogasawara, T., Nakai, A., and Kasuya, T., "Effect of solidity on aerodynamic forces around straight-bladed vertical axis wind turbine by wind tunnel experiments (depending on number of blades)," *Renewable Energy*, Vol. 96, No. Part A, Oct. 2016, pp. 928–939.

[12]Kanner, S. and Persson, P.-O., "Validation of a High-Order Large-Eddy Simulation Solver Using a Vertical-Axis Wind Turbine," *AIAA Journal*, 2015.

[13]Froehle, B. M., *High-Order Discontinuous Galerkin Fluid-Structure Interaction Methods*, Ph.D. thesis, University of California, Berkeley, 2013.

[14]Chorin, A. J., "A numerical method for solving incompressible viscous flow problems [J. Comput. Phys. **2** (1967), no. 1, 12–36]," *J. Comput. Phys.*, Vol. 135, No. 2, 1997, pp. 115–125, With an introduction by Gerry Puckett, Commemoration of the 30th anniversary {of J. Comput. Phys.}.

[15]Persson, P.-O., Bonet, J., and Peraire, J., "Discontinuous Galerkin solution of the Navier-Stokes equations on deformable domains," *Comput. Methods Appl. Mech. Engrg.*, Vol. 198, No. 17–20, 2009, pp. 1585–1595.

[16]Hesthaven, J. S. and Warburton, T., *Nodal discontinuous Galerkin methods*, Vol. 54 of *Texts in Applied Mathematics*, Springer, New York, 2008, Algorithms, analysis, and applications.

[17]Peraire, J. and Persson, P.-O., "High-order discontinuous Galerkin methods for CFD," *Adaptive high-order methods in computational fluid dynamics*, Vol. 2 of *Adv. Comput. Fluid Dyn.*, World Sci. Publ., Hackensack, NJ, 2011, pp. 119–152.

[18]Roe, P. L., "Approximate Riemann solvers, parameter vectors, and difference schemes," *J. Comput. Phys.*, Vol. 43, No. 2, 1981, pp. 357–372.

[19]Peraire, J. and Persson, P.-O., "The compact discontinuous Galerkin (CDG) method for elliptic problems," *SIAM J. Sci. Comput.*, Vol. 30, No. 4, 2008, pp. 1806–1824.

[20]Pazner, W. and Persson, P.-O., "Stage-parallel fully implicit Runge-Kutta solvers for discontinuous Galerkin fluid simulations," *J. Comput. Phys.*, Vol. 335, 2017, pp. 700–717.

[21]Persson, P.-O., "Scalable Parallel Newton-Krylov Solvers for Discontinuous Galerkin Discretizations," *47th AIAA Aerospace Sciences Meeting and Exhibit, Orlando, Florida*, 2009, AIAA-2009-606.

[22]The OpenFOAM Foundation, *OpenFOAM v5 User Guide*.

[23]Holzmann, T., "Mathematics, Numerics, Derivations and OpenFOAM(R)," Tech. rep., Leoben, Feb. 2017.

[24]Moukalled, F., Mangani, L., and Darwish, M., *The finite volume method in computational fluid dynamics*, Springer, Cham, Switzerland, 2016.

[25]ISSA, R. I., "Solution of Implicitly Discretized Fluid Flow Equations by Operator Splitting," *J. Comput. Phys.*, Vol. 62, 1986, pp. 40.

[26]Li, Q., Maeda, T., Kamada, Y., Murata, J., Kawabata, T., Shimizu, K., Ogasawara, T., Nakai, A., and Kasuya, T., "Wind tunnel and numerical study of a straight-bladed vertical axis wind turbine in three-dimensional analysis (Part I: For predicting aerodynamic loads and performance)," *Energy*, Vol. 106, No. Supplement C, July 2016, pp. 443–452.